Searching for Dark Matter with a Superconducting Qubit

Akash V. Dixit[1,2,3,+], Srivatsan Chakram[1,2], Kevin He[1,2], Ankur Agrawal[1,2,3], Ravi K. Naik[4], David I. Schuster[1,2,5], and Aaron Chou[6]

[1] *Department of Physics, University of Chicago, Chicago, Illinois 60637, USA*
[2] *James Franck Institute, University of Chicago, Chicago, Illinois 60637, USA*
[3] *Kavli Institute for Cosmological Physics, University of Chicago, Chicago, Illinois 60637, USA*
[4] *Department of Physics, University of California Berkeley, California 94720, USA.*
[5] *Pritzker School of Molecular Engineering, University of Chicago, Chicago, Illinois 60637, USA*
[6] *Fermi National Accelerator Laboratory, Batavia, Illinois 60510, USA*
[+] Correspondence to: avdixit@uchicago.edu

The gravitational evidence for the existence of dark matter is extensive, yet thus far, dark matter has evaded direct detection in terrestrial experiments. Detection mechanisms for low mass dark matter candidates such as the axion [1–4] or hidden photon [5,6] leverage potential interactions with electromagnetic fields, whereby the dark matter (of unknown mass) on rare occasion converts into a single photon [7,6]. Current dark matter searches operating at microwave frequencies, use a resonant cavity to coherently accumulate the field sourced by the dark matter and use a quantum limited linear amplifier to read out the cavity signal [8–11]. Here, we report the development of a novel microwave photon counting technique and use it to set a new exclusion limit on hidden photon dark matter. We constrain the kinetic mixing angle to $\epsilon \leq 1.82 \times 10^{-15}$ in a narrow band around 6.011 GHz (24.86 μeV) with an integration time of 8.33 s. We operate a superconducting qubit to make repeated quantum non-demolition measurements of cavity photons and apply a hidden Markov model analysis to reduce the noise to 15.7 dB below the quantum limit, with performance limited by the residual population of the system. The techniques presented here will dramatically improve the sensitivity of future dark matter searches in the range of 3-30 GHz and are generally applicable to measurements that require high sensitivity to inherently low signal photon rates.

The nature of dark matter is an enduring mystery of our universe. Dark matter comprises 26.5% of the energy-matter content in the universe and is five times more abundant than visible matter [12]. Observations of galaxy rotation curves, gravitational lensing, and the presence of structure in the cosmos all inform our understanding of dark matter, but provide little insight into its intrinsic properties [13].

We are interested in testing the hypothesis that dark matter is composed of waves of low mass bosons, which due to their high galactic phase space density, arrive as coherent waves with macroscopic occupation number. Well known dark matter candidates include the axion and hidden sector photon, which both have compelling cosmological origin stories [1–6].

One method for detecting these dark matter waves exploits their interactions with the electromagnetic field [7,6]. The dark matter candidate forms an effective oscillating current density that sources Maxwell's equations. For axions, the effective current density is $\mathbf{j}_{\text{axion}} = g_{a\gamma\gamma}\sqrt{2\rho}\mathbf{B}_0 e^{im_a t}$, where $g_{a\gamma\gamma}$ is the predicted coupling of the axion field to electromagnetism, ρ is the local dark matter density, $\mathbf{B}_0$ is a DC magnetic field applied in the laboratory, and m_a is the mass of the axion. For hidden photons, the effective current is $\mathbf{j}_{\text{HP}} = \epsilon m_{\gamma'}\sqrt{2\rho}e^{im_{\gamma'}t}\hat{\mathbf{n}}$, where ϵ is a postulated kinetic angle of mixing between standard electromagnetism and hidden sector electromagnetism, $\hat{\mathbf{n}}$ is the polarization of the hidden photon field, and $m_{\gamma'}$ is the hidden photon mass. Via Faraday's law, the electric field of a microwave cavity is sourced by the effective current formed by the dark matter $\nabla \times \mathbf{B} - \frac{\partial \mathbf{E}}{\partial t} = \mathbf{j}_{\text{DM}}$. A microwave cavity with resonance frequency tuned to the mass of the hypothetical particle is then used to coherently accumulate the electromagnetic response.

There are specified targets in the parameter space of coupling and dark matter mass in the case of the axion of quantum chromodynamics. The expected signal photon occupation number is $\sim 10^{-2}$ for searches like the Axion Dark Matter eXperiment operating at 650 MHz [8]. However, the microwave cavity volume must shrink at higher frequencies to maintain the resonance condition. The signal photon rate scales with the volume of the cavity, making detection of smaller signals increasingly challenging at higher frequencies. For an axion search with the microwave cavity (6.011 GHz) used in the present work and given the experimental parameters in typical axion search experiments [9–11], the axion models (DFSZ and KSVZ) [14–17] predict a signal with mean photon number of $\bar{n}_{\text{axion}} \sim 10^{-8} - 10^{-5}$ per measurement. For hidden photons, the parameter space is less constrained, [5,18] and the mean photon number per measurement could be $\bar{n}_{\text{HP}} \leq 10^{-1}$. Currently, these searches employ linear amplification operating near the standard quantum limit (SQL) [19] to read out the built up signal in the microwave cavity, where the noise variance is equivalent to fluctuations of an effective background of $\bar{n}_{\text{noise}} = 1$. At GHz frequencies and above, the noise inherent to quantum limited linear amplification overwhelms the signal, making the search untenable ($\bar{n}_{\text{noise}} \gg \bar{n}_{\text{axion}}, \bar{n}_{\text{HP}}$).

Counting photons to detect Dark Matter

We use single photon resolving detectors to avoid quantum noise by measuring only field amplitude resulting in insensitivity to the conjugate phase observable. The noise is then dominated by the Poisson fluctuations of the background counts and ultimately limited by the shot noise of the signal itself [20]. Technologies such as super-

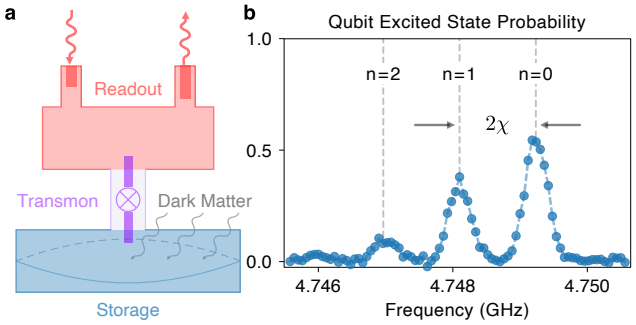

Fig. 1: Superconducting transmon qubit dispersively coupled to high Q storage cavity. **a,** Schematic of photon counting device consisting of storage and readout cavities bridged by a transmon qubit[26]. The interaction between the dark matter and electromagnetic field results in a photon being deposited in the storage cavity. **b,** Qubit spectroscopy reveals that the storage cavity population is imprinted as a shift of the qubit transition frequency. The photon number dependent shift is 2χ per photon.

conducting nanowire single-photon detectors or photomultipier tubes can readily count photons with virtually no background counts for terahertz frequency photons. However, these technologies are not well suited to detect single low energy microwave photons[21]. We aim to develop a detector that is sensitive in the microwave regime and has a low dark count probability commensurate with the small signal rates expected in a dark matter experiment.

In order to construct such a single photon counter, we build from the work of Haroche et. al. in coupling atomic systems to electromagnetic fields[22,23]. Here, we utilize the interaction between a superconducting transmon qubit[24] and the field in a microwave cavity to count photons. In the dispersive limit (qubit-cavity coupling $\ll$ qubit, cavity detuning), the Jaynes-Cummings Hamiltonian[25] describes the interactions between a qubit and cavity, and is expressed as $\mathcal{H}/\hbar = \omega_c a^\dagger a + \frac{1}{2}\omega_q \sigma_z + 2\chi a^\dagger a \frac{1}{2}\sigma_z$. The Hamiltonian can be recast to elucidate a key feature: a photon number dependent frequency shift (2χ) of the qubit transition (Fig. 1b).

$$\mathcal{H}/\hbar = \omega_c a^\dagger a + \frac{1}{2}(\omega_q + 2\chi a^\dagger a)\sigma_z \qquad (1)$$

We use an interferometric Ramsey measurement of the qubit frequency to infer the cavity state[27]. Qubit decay, dephasing, heating, cavity decay, and readout infidelity are the main sources of errors in this measurement. The qubit-cavity interaction ($2\chi a^\dagger a \frac{1}{2}\sigma_z$) is composed solely of number operators and commutes with the bare Hamiltonian of the cavity ($\omega_c a^\dagger a$) and qubit ($\frac{1}{2}\omega_q \sigma_z$). Thus, the cavity photon state collapses to a Fock state ($|0\rangle$ or $|1\rangle$ in the $n \ll 1$ limit) upon measurement, rather than being absorbed and destroyed[28–31]. Crucially, this allows us to repeat the photon number measurement multiple times. We devise a counting protocol insensitive to any individual measurement error[32–34], dramatically reducing the probability of false positives.

Instead of producing amplitude noise like a SQL amplifier, the backaction associated with quantum nondemolition (QND) counting of single photons is the complete randomization of the phase of the electromagnetic field in the cavity, due to the number phase uncertainty relation. However, the phase information is not necessary to determine if the dark matter wave has successfully deposited a photon in the cavity. This QND technique provides the means necessary to achieve the sub-SQL noise required to detect dark matter.

In this work, we use a device composed of a high quality factor ($Q_s = 2.06 \times 10^7$) 3D cavity used to accumulate and store the signal induced by the dark matter (storage, $\omega_s = 2\pi \times 6.011\,\mathrm{GHz}$), a superconducting transmon qubit ($\omega_q = 2\pi \times 4.479\,\mathrm{GHz}$), and a 3D cavity strongly coupled to a transmission line ($Q_r = 1.5 \times 10^4$) used to quickly read out the state of qubit (readout, $\omega_r = 2\pi \times 8.051\,\mathrm{GHz}$) (Fig. 1a). We mount the device to the base stage of a dilution refrigerator at 8 mK (see Supplementary Information sections A, B, C).

To count photons, we map the cavity population onto the qubit state by performing a cavity number parity measurement with Ramsey interferometry. This is accomplished by placing the qubit, initialized either in $|g\rangle$ or $|e\rangle$, in a superposition state $\frac{1}{\sqrt{2}}(|g\rangle \pm |e\rangle)$ with a $\pi/2$ pulse. The qubit state precesses at a rate of $2\chi = 2\pi \times 1.13\,\mathrm{MHz}$ when there is one photon in the storage cavity due to the photon dependent shift of the qubit frequency. Waiting for a time $t_p = \pi/(2\chi)$ results in the qubit state accumulating a π phase if there is one photon in the cavity. We project the qubit back onto the z-axis with a $-\pi/2$ pulse completing the mapping of the storage cavity photon number onto the qubit state. If there were zero photons in the cavity, the qubit remains in its initial state. If there were one photon in the cavity the qubit state is flipped ($|g\rangle \leftrightarrow |e\rangle$) (see Supplementary Information section D). We then determine the qubit state using it's standard dispersive coupling to the readout resonator. The parity measurement is depicted in Fig. 2a. For weak cavity displacements ($\bar{n} \ll 1$), this protocol functions as a qubit π pulse conditioned on the presence of a single cavity photon[27]. Qubit and readout errors during the parity measurement introduce inefficiencies or worse, false positive detections. For contemporary transmon qubits, these errors occur with much greater probability (1-10%) than the appearance of a dark matter induced photon, resulting in a measurement that is limited by detector errors. To suppress the detector errors, we make repeated QND measurements of the cavity population, as shown in Fig. 2a[32–34].

Hidden Markov model analysis

In order to account for all possible error mechanisms during the measurement protocol, we model the evolution of the cavity, qubit, and readout as a hidden Markov process where the cavity and qubit states are hidden variables that emit as a readout signal (see Fig. 2b). The Markov chain is characterized by the transition matrix

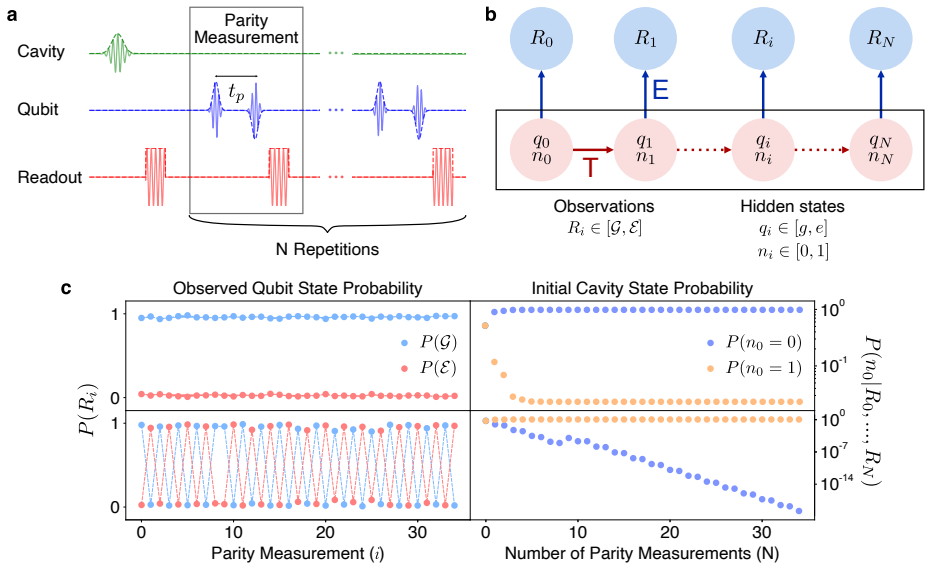

Fig. 2: Photon counting protocol and hidden Markov model analysis. **a,** Pulse sequence for photon counting includes cavity initialization and repeated parity measurements, consisting of a $\pi/2$ pulse, a wait time of t_p, and a $-\pi/2$ pulse followed by a qubit readout. **b,** Cavity and qubit states evolve under transition matrix T, readout measurements are governed by emission matrix E. **c,** (Left) Sequence of qubit readout signals for two events. (Right) Reconstructed initial cavity photon state probabilities. The probability of a detector error resulting in a false positive are exponentially suppressed when multiple successful flips are observed.

(T) (Equation 2) that governs how the joint cavity, qubit hidden state $s \in [|0g\rangle, |0e\rangle, |1g\rangle, |1e\rangle]$ evolve, and the emission matrix (E) (Equation 3) which determines the probability of a readout signal R $\in [\mathcal{G},\mathcal{E}]$ given a possible hidden state.

$$T = \begin{array}{c} \begin{matrix} |0g\rangle & |0e\rangle & |1g\rangle & |1e\rangle \end{matrix} \\ \begin{bmatrix} P_{00}P_{gg} & P_{00}P_{ge} & P_{01}P_{gg} & P_{01}P_{ge} \\ P_{00}P_{eg} & P_{00}P_{ee} & P_{01}P_{eg} & P_{01}P_{ee} \\ P_{10}P_{gg} & P_{10}P_{ge} & P_{11}P_{ge} & P_{11}P_{gg} \\ P_{10}P_{eg} & P_{10}P_{ee} & P_{11}P_{ee} & P_{11}P_{eg} \end{bmatrix} \end{array} \begin{matrix} |0g\rangle \\ |0e\rangle \\ |1g\rangle \\ |1e\rangle \end{matrix} \quad (2)$$

We determine the elements of the transition matrix using independently measured qubit coherences ($T_1^q = 108 \pm 18\,\mu s$, $T_2^q = 61 \pm 4\,\mu s$), cavity lifetime ($T_1^s = 546 \pm 23\,\mu s$), qubit spurious excited state population ($\bar{n}_q = 5.1 \pm 0.3 \times 10^{-2}$), the length of the parity measurement ($t_p = 380\,ns$) (see Supplementary Information section F.1), and the time between parity measurements ($t_m = 10\,\mu s$). The repetition rate of the experiment is constrained primarily by the readout time ($3\,\mu s$) and time for the readout resonator to relax back to the ground state. Qubit (cavity) relaxation $|e\rangle \rightarrow |g\rangle$ ($|1\rangle \rightarrow |0\rangle$) occurs with a probability $P_{eg}^{\downarrow} = 1 - e^{-t_m/T_1^q}$ ($P_{10} = 1 - e^{-t_m/T_1^s}$). The probability of spontaneous heating $|g\rangle \rightarrow |e\rangle$ ($|0\rangle \rightarrow |1\rangle$) of the qubit (cavity) towards its steady state population is given by $P_{ge}^{\uparrow} = \bar{n}_q[1 - e^{-t_m/T_1^q}]$ ($P_{01} = \bar{n}_c[1 - e^{-t_m/T_1^s}]$). $\bar{n}_c$ is set to zero in the model in order to penalize events in which a photon appears in the cavity after the measurement sequence has begun (see Supplementary Information section G.2). This makes the detector insensitive to cavity heating events. Dephasing during the parity measurement occurs with probability $P^{\phi} = 1 - e^{-t_p/T_2^q}$, leading to outcomes indistinguishable from qubit heating or decay. The transition matrix contains all qubit errors: $P_{ge} = P_{ge}^{\uparrow} + P^{\phi}$ and $P_{eg} = P_{eg}^{\downarrow} + P^{\phi}$. P_{gg}, P_{ee}, P_{00}, and P_{11} correspond to events where no error occurs, such that probabilities pairwise sum to unity (e.g. $P_{gg} + P_{ge} = 1$).

$$E = \frac{1}{2} \begin{array}{c} \begin{matrix} \mathcal{G} & \mathcal{E} \end{matrix} \\ \begin{bmatrix} F_{g\mathcal{G}} & F_{g\mathcal{E}} \\ F_{e\mathcal{G}} & F_{e\mathcal{E}} \\ F_{g\mathcal{G}} & F_{g\mathcal{E}} \\ F_{e\mathcal{G}} & F_{e\mathcal{E}} \end{bmatrix} \end{array} \begin{matrix} |0g\rangle \\ |0e\rangle \\ |1g\rangle \\ |1e\rangle \end{matrix} \quad (3)$$

The elements of the emission matrix are composed of the independently measured readout fidelities of the ground and excited states of the qubit ($F_{g\mathcal{G}} = 95.8 \pm 0.4\,\%, F_{e\mathcal{E}} = 95.3 \pm 0.5\,\%$). Noise from the first stage cryogenic HEMT amplifier sets the readout fidelity (see Supplementary Information section F.2).

Given a set of N+1 measured readout signals $(R_0, R_1, ..., R_N)$, we reconstruct the initial cavity state probabilities $P(n_0 = 0)$ and $P(n_0 = 1)$ by using the backward algorithm[32,33] and summing over all possible initial qubit states, as shown in Equation 4.

$$P(n_0) = \sum_{s_0 \in [|n_0,g\rangle, |n_0,e\rangle]} \sum_{s_1} ... \sum_{s_N} E_{s_0,R_0} T_{s_0,s_1} E_{s_1,R_1} \\ ...T_{s_{N-1},s_N} E_{s_N,R_N} \quad (4)$$

This reconstruction includes terms corresponding to all the possible processes that could occur. For example, a readout measurement of $\mathcal{G}$ followed by $\mathcal{E}$ could occur due the correct detection of a photon in the cavity (with probability $P_{11}P_{gg}F_{e\mathcal{E}}/2$). Alternatively, this measurement could be produced by a qubit heating event ($P_{00}P_{ge}F_{e\mathcal{E}}/2$) or a readout error ($P_{00}P_{gg}F_{g\mathcal{E}}/2$). Fig. 2c displays the measured readout signals and reconstructed initial cavity probabilities of two events. The top panels correspond to the absence of a cavity photon and the bottom panels indicate the presence of a photon.

We apply a likelihood ratio test ($\lambda = \frac{P(n_0=1)}{P(n_0=0)}$) to the reconstructed cavity state probabilities to determine

if the cavity contained zero or one photons. If the likelihood ratio is greater than (less than) a threshold, $\lambda > \lambda_{\rm thresh}$ ($\lambda \leq \lambda_{\rm thresh}$), we determine the cavity to contain one (zero) photon. The probability of a false positive detection due to detector errors is therefore less than $\frac{1}{\lambda_{\rm thresh}+1}$. As the threshold for detection increases, so too does the number of repeated parity measurements needed to confirm the presence of a photon. This protocol and analysis exacts a cost to detection efficiency that is linear in the number of measurements (see Supplementary Information section G.1). More importantly for the detection of rare events, the suppression of false positives grows exponentially with more repeated measurements, as evident in Fig. 2c.

Detector characterization

To characterize the detector, we populate the cavity by applying a weak drive ($\bar{n} \ll 1$) (see Supplementary Information section E). We map out the relationship between the probability of injected and measured photons (Fig. 3a) by varying the injected mean photon population ($\bar{n} = \alpha^2$), performing 30 repeated parity measurements, and applying $\lambda_{\rm thresh}$ to discriminate between one and zero photon events. We fit this relationship to obtain the efficiency of detection (η) and the false positive probability (δ). False positives occur when the detector determines that a photon is present in the cavity even when no photon is injected.

Fig. 3b show that as we increase the likelihood threshold $\lambda_{\rm thresh}$, the efficiency corrected false positive probability (δ/η) initially decreases, but eventually asymptotes. The initial decrease for low thresholds indicates a suppression of false positives due to detector errors. Leveling off at larger thresholds indicates that the dominant source of false positives is no longer detector errors, but rather a background of real photons.

False positives that occur when qubit errors are highly suppressed (at large $\lambda_{\rm thresh}$) are due to a photon background in the storage cavity. We measure the cavity occupation to be $\bar{n}_c = 7.3 \pm 2.9 \times 10^{-4}$, corresponding to a temperature of 39.9 ± 2.2 mK. In experiments with no photons injected into the cavity, we observe events with likelihood ratios comparable with those seen in experiments with injected photons (Fig. 3c). The detector thus correctly identifies real photons which, in the regime of highly suppressed detector errors, set the background for dark matter searches.

The cavity photon temperature (39.9 ± 2.2 mK) is greater than the physical temperature of the device (8 mK) indicating coupling to extraneous baths. One contribution, arising from coupling to quasiparticles via qubit dressing of the cavity[35], results in a photon population of $\bar{n}_c^q = 1.8 \pm 0.1 \times 10^{-4}$ (see Supplementary Information section H). Suppression of quasiparticle production could be achieved by enhanced infrared filtering, extensive radiation shielding, gap engineering, and quasiparticle trapping[36–38]. Other sources of background photons could include blackbody radiation from higher temperature stages of the dilution refrigerator, poorly thermalized or insufficiently attenuated microwave lines, or amplifier noise[39,40]. With further reduction of the background population down to the physical temperature of 8 mK, we can achieve a background free search for dark matter.

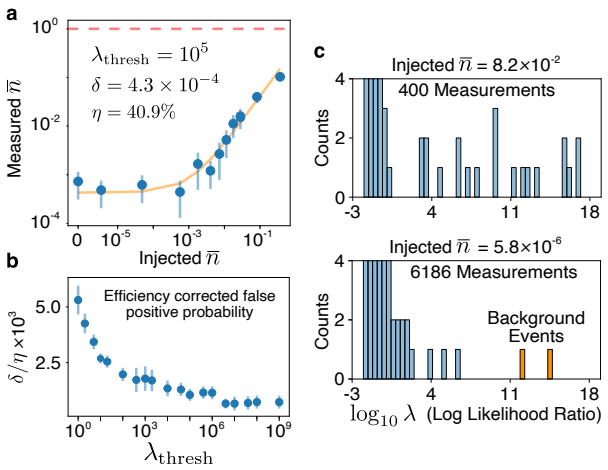

Fig. 3: Detector characterization. **a,** After a variable initial cavity displacement, 30 repeated parity measurements of cavity photon state are performed and a threshold $\lambda_{\rm thresh}$ is applied to determine the cavity population. Detector efficiency (η) and false positive probability (δ) are determined from the fit (in orange). Counting photons results in a three order of magnitude advantage over quantum limited amplification operating in phase insensitive mode (dashed red). **b,** The efficiency corrected false positive probability (δ/η) vs threshold ($\lambda_{\rm thresh}$) curve asymptotes at high thresholds, indicating qubit errors are now a sub dominant contribution to the total detector false positive probability. **c,** Histograms of log likelihood ratios of all events for two different injected mean photon numbers. The histogram y-axis is cut off at 4 counts to view the rare events at high log likelihood ratios. We observe unexpected photon events when very small photon numbers are injected with log likelihood ratios similar to that expected from real injected photon events. These events are interpreted as real background photons occupying the storage cavity rather than detector error based false positives.

Hidden Photon Dark Matter exclusion

By counting photons with repeated parity measurements and applying a Markov model based analysis, we demonstrate single photon detection with amplitude noise equivalent to $-10\log_{10}\sqrt{\bar{n}_c} = 15.7 \pm 0.9$ dB below the quantum limit. We use this detector to conduct a narrow band hidden photon search. We collect 15,141 measurements where the injected $\bar{n}$ is well below the background population $\bar{n}_c$. Each measurement consists of integrating the signal (for the cavity lifetime, $T_1^s = 546\,\mu$s) and counting the number of photons in the cavity with 30 repeated parity measurements ($30 \times t_m = 300\,\mu$s). The total search time is $15{,}141 \times (546 + 300)\mu$s $= 12.81$ s with a duty cycle of $\frac{546\mu s}{846\mu s} = 65\%$. We apply a detection threshold of $\lambda_{\rm thresh} = 10^5$, such that the qubit errors are suppressed below the background photon probability

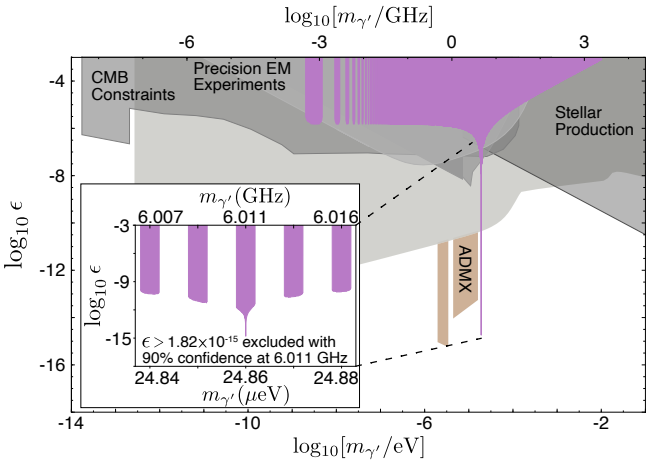

Fig. 4: Hidden Photon Dark Matter parameter space. Shaded regions in the hidden photon parameter space[5,6] of coupling (ϵ) and mass (m_γ) are excluded. The exclusion set with the qubit based photon counting search presented in this work, is shown in purple. The detector is most sensitive on resonance with the storage cavity ($m_{\gamma'}c^2 = \hbar\omega_s$) and the hidden photon kinetic mixing angle is constrained to $\epsilon \leq 1.82 \times 10^{-15}$ at 90% confidence. We perform repeated measurements of the number parity of the cavity state, so the detector is sensitive to cavity populations that have weight in the odd cavity states greater than the measured background. The detector sensitivity is dependent on the mass of the dark matter candidate, giving rise to bands of exclusion (see inset) centered around regions where the cavity number dependent qubit shift[41] is an odd multiple of 2χ (see Supplementary Information section J).

($\frac{1}{\lambda_{\text{thresh}}+1} < \bar{n}_c$), resulting in the detector operating with a quantum efficiency of $\eta = 40.9\%$ (Fig. 3a). Accounting for the efficiency of the detector, we count 22 photons. A hidden photon candidate with coupling (ϵ) and mass ($m_{\gamma'}$) that on average produces more than 29.3 photons in 15,141 measurements is therefore excluded at the 90% confidence level (see Supplementary Information section I). Fig. 4 shows the region of hidden photon parameter space excluded by the qubit based search. The detector is maximally sensitive to dark matter candidates with masses within a narrow window around the resonance frequency of the cavity. Sensitivity to off resonant candidates occurs in regions where the photon number dependent qubit shift is an odd multiple of 2χ (see Supplementary Information section J). The hidden photon mixing angle is constrained to $\epsilon \leq 1.82 \times 10^{-15}$ with 90% confidence for hidden photon candidates with mass equal to the resonance frequency of the storage cavity ($m_{\gamma'}c^2 = \hbar\omega_s$).

Future Dark Matter searches

The photon detection technique developed in this work has unprecedented sensitivity to dark matter candidates and enables future cavity based searches for axions and hidden photons in the 3-30 GHz range.

In order to implement a full scale axion search, the photon counting device must be coupled to a microwave cavity bathed in a magnetic field that accumulates the axion deposited signal. To extract the signal, a nonlinear element such as a Josephson parametric converter can be used to transfer the signal photon from the accumulation cavity to the storage cavity[42,43]. When the accumulation cavity frequency is tuned to search for a different axion mass, the converter can be pumped at appropriate frequency to enable photon transfer. The storage cavity and qubit can remain fixed in frequency, which leaves the photon detection protocol unchanged at each tuning.

Although novel cavity techniques to achieve high Q in the presence of magnetic fields have been demonstrated[44], in the most pessimistic scenario the accumulation cavity will be made of copper and limited to a $Q \sim 10^4$ at 10 GHz due to the anomalous skin effect. This sets the accumulation time to $\sim 1\,\mu$s. To minimize the dead time of the experiment, the time required to measure the storage cavity should ideally be matched to that of a copper accumulation cavity lifetime. Reaching the required detector error probability in this limited time will be challenging. In this work, each parity measurement requires 10 µs because of the large readout signal necessary to overcome the HEMT amplifier noise. We perform 30 repeated measurements in order to reduce the probability of detector errors to a level below the expected signal photon probability for dark matter ($\bar{n}_{\text{axion}} \sim 10^{-8}$). Readout of a superconducting qubit with $> 99\%$ fidelity in 100 ns has been achieved by using quantum limited parametric amplifiers[45] and appropriate pulse shaping[46]. Both techniques can be applied to this protocol to significantly increase the measurement rate and readout fidelity.

For a hidden photon search, a magnetic field is not required. As demonstrated in this work, the accumulation and storage cavity can be the same device. When the cavity is tuned to search through the parameter space, as long as a sufficiently large stark shift to the accumulation/storage is maintained and the qubit is still far detuned, the fundamental QND interaction between the qubit and photon is maintained.

Application in quantum computing

Counting photons will also be a useful tool for quantum computing architectures which utilize long lived storage cavities[47,48] that are sensitive to residual cavity population. Though qubit dephasing is typically used to calibrate the background photon population of the system, this technique is only sensitive to the low Q readout cavity and not the storage cavity which has a much longer lifetime than the qubit. Alternatively, the storage cavity population can be extracted by driving Rabi oscillations of the 2χ shifted qubit transition, but this yields only the average cavity photon number over multiple experimental runs. Counting photons with repeated measurements to assess the cavity population independently of the qubit errors allows for both single shot and real time monitoring of the storage cavity, crucial when preparing

states whose fidelity is sensitive to the initial conditions.

Conclusions

Photon number measurements allow us to gain unprecedented sensitivity to dark matter signals. The single photon counting protocol demonstrated in this work constitutes a 1.4×10^3 improvement of the dark count rate (15.7 dB in amplitude), relative to the zero point noise added by a quantum limited amplifier. This improvement is currently limited by background photons whose suppression will further increase the sensitivity of the detector. Dark matter searches in the mass range of 3-30 GHz can be performed by a series of tuned narrow band measurements with the detector sensitivities achieved in this work. We demonstrate that qubit based counting technology is readily applicable to current narrow band experiments by performing a hidden photon dark matter search and excluding candidates with mixing angle $\epsilon > 1.82 \times 10^{-15}$ in a band around 6.011 GHz. To extend the detection scheme presented in this work to searches beyond 30 GHz, a nonlinear element with a higher plasma frequency than that of Aluminium, such as Tantalum [49], Niobium, or Titanium Nitride, could be used. For dark matter searches in the mass range of 10-100 µeV, qubit based photon counting is the enabling technology.

Data Availability

The experimental data and analysis presented in this manuscript are available from the corresponding author upon request.

References

[1] Peccei, R. D. & Quinn, H. R. CP conservation in the presence of pseudoparticles. *Phys. Rev. Lett.* (1977).

[2] Peccei, R. D. & Quinn, H. R. Constraints imposed by CP conservation in the presence of pseudoparticles. *Phys. Rev. D* (1977).

[3] Weinberg, S. A New Light Boson? *Phys. Rev. Lett.* **40**, 223–226 (1978).

[4] Wilczek, F. Problem of Strong P and T Invariance in the Presence of Instantons. *Phys. Rev. Lett.* **40**, 279–282 (1978).

[5] Arias, P. *et al.* Wispy cold dark matter. *Journal of Cosmology and Astroparticle Physics* **2012**, 013–013 (2012).

[6] Graham, P. W., Mardon, J. & Rajendran, S. Vector dark matter from inflationary fluctuations. *Phys. Rev. D* **93** (2016).

[7] Sikivie, P. Experimental tests of the "invisible" axion. *Phys. Rev. Lett.* **51**, 1415–1417 (1983).

[8] Du, N. *et al.* Search for Invisible Axion Dark Matter with the Axion Dark Matter Experiment. *Phys. Rev. Lett.* **120**, 151301 (2018).

[9] Braine, T. *et al.* Extended search for the invisible axion with the axion dark matter experiment. *Phys. Rev. Lett.* **124** (2020).

[10] Brubaker, B. M. *et al.* First Results from a Microwave Cavity Axion Search at 24 μeV. *Phys. Rev. Lett.* **118**, 1–5 (2017).

[11] Zhong, L. *et al.* Results from phase 1 of the haystac microwave cavity axion experiment. *Phys. Rev. D* **97** (2018).

[12] Tanabashi, M. *et al.* Review of particle physics. *Phys. Rev. D* **98**, 030001 (2018).

[13] Rubin, V. C., Ford, J., W. K. & Thonnard, N. Rotational properties of 21 SC galaxies with a large range of luminosities and radii, from NGC 4605 (R=4kpc) to UGC 2885 (R=122kpc). *Astrophysical Journal* **238**, 471–487 (1980).

[14] Dine, M., Fischler, W. & Srednicki, M. A simple solution to the strong CP problem with a harmless axion. *Physics Letters B* **104**, 199–202 (1981).

[15] Zhitnitsky, A. On Possible Suppression of the Axion Hadron Interactions. (In Russian). *Sov. J. Nucl. Phys.* **31**, 260 (1980).

[16] Kim, J. E. Weak-interaction singlet and strong CP invariance. *Phys. Rev. Lett.* **43**, 103–107 (1979).

[17] Shifman, M., Vainshtein, A. & Zakharov, V. Can confinement ensure natural cp invariance of strong interactions? *Nuclear Physics B* **166**, 493–506 (1980).

[18] Horns, D. *et al.* Searching for wispy cold dark matter with a dish antenna. *Journal of Cosmology and Astroparticle Physics* **2013**, 016–016 (2013).

[19] Caves, C. M. Quantum limits on noise in linear amplifiers. *Phys. Rev. D* **26**, 1817–1839 (1982).

[20] Lamoreaux, S. K., van Bibber, K. A., Lehnert, K. W. & Carosi, G. Analysis of single-photon and linear amplifier detectors for microwave cavity dark matter axion searches. *Phys. Rev. D* **88**, 35020 (2013).

[21] Hadfield, R. Single-photon detectors for optical quantum information applications. *Nature Photonics* **3**, 696–705 (2009).

[22] Brune, M., Haroche, S., Lefevre, V., Raimond, J. M. & Zagury, N. Quantum nondemolition measurement of small photon numbers by rydberg-atom phase-sensitive detection. *Phys. Rev. Lett.* **65**, 976–979 (1990).

[23] Gleyzes, S. *et al.* Observing the quantum jumps of light : birth and death of a photon in a cavity. *Nature* **446**, 297 (2007).

[24] Koch, J. *et al.* Charge-insensitive qubit design derived from the cooper pair box. *Phys. Rev. A* **76** (2007).

[25] Jaynes, E. T. & Cummings, F. W. Comparison of quantum and semiclassical radiation theories with application to the beam maser. *Proceedings of the IEEE* **51**, 89–109 (1963).

[26] Leek, P. J. *et al.* Cavity quantum electrodynamics with separate photon storage and qubit readout modes. *Phys. Rev. Lett.* **104** (2010).

[27] Kono, S., Koshino, K., Tabuchi, Y., Noguchi, A. & Nakamura, Y. Quantum non-demolition detection of an itinerant microwave photon. *Nature Physics* **14**, 546–549 (2018).

[28] Braginsky, V. B. & Khalili, F. Y. Quantum nondemolition measurements: the route from toys to tools. *Rev. Mod. Phys.* **68**, 1–11 (1996).

[29] Nogues, G. *et al.* Seeing a single photon without destroying it. *Nature* **400**, 239–242 (1999).

[30] Johnson, B. R. *et al.* Quantum non-demolition detection of single microwave photons in a circuit. *Nature Physics* **6**, 663–667 (2010).

[31] Sun, L. *et al.* Tracking photon jumps with repeated quantum non-demolition parity measurements. *Nature* **511**, 444–448 (2014).

[32] Zheng, H., Silveri, M., Brierley, R. T., Girvin, S. M. & Lehnert, K. W. Accelerating dark-matter axion searches with quantum measurement technology. *arXiv:1607.02529* (2016).

[33] Hann, C. T. *et al.* Robust readout of bosonic qubits in the dispersive coupling regime. *Phys. Rev. A* **98** (2018).

[34] Elder, S. S. *et al.* High-fidelity measurement of qubits encoded in multilevel superconducting circuits. *Phys. Rev. X* **10** (2020).

[35] Serniak, K. *et al.* Hot nonequilibrium quasiparticles in transmon qubits. *Phys. Rev. Lett.* **121** (2018).

[36] Christensen, B. G. *et al.* Anomalous charge noise in superconducting qubits. *Phys. Rev. B* **100** (2019).

[37] Vepsäläinen, A. *et al.* Impact of ionizing radiation on superconducting qubit coherence. *arXiv:2001.09190* (2020).

[38] Riwar, R.-P. *et al.* Normal-metal quasiparticle traps for superconducting qubits. *Physical Review B* **94** (2016).

[39] Yeh, J.-H., LeFebvre, J., Premaratne, S., Wellstood, F. C. & Palmer, B. S. Microwave attenuators for use with quantum devices below 100 mk. *Journal of Applied Physics* **121**, 224501 (2017).

[40] Wang, Z. *et al.* Cavity attenuators for superconducting qubits. *Phys. Rev. Appl.* **11** (2019).

[41] Gambetta, J. *et al.* Qubit-photon interactions in a cavity: Measurement-induced dephasing and number splitting. *Phys. Rev. A* **74**, 042318 (2006).
[42] Axline, C. J. *et al.* On-demand quantum state transfer and entanglement between remote microwave cavity memories. *Nature Physics* **14**, 705–710 (2018).
[43] Leung, N. *et al.* Deterministic bidirectional communication and remote entanglement generation between superconducting quantum processors. *npj Quantum Information* **5** (2018).
[44] Alesini, D. *et al.* High quality factor photonic cavity for dark matter axion searches. *arXiv:2002.01816* (2020).
[45] Walter, T. *et al.* Rapid high-fidelity single-shot dispersive readout of superconducting qubits. *Phys. Rev. Appl.* **7** (2017).
[46] McClure, D. *et al.* Rapid driven reset of a qubit readout resonator. *Phys. Rev. Appl.* **5** (2016).
[47] Naik, R. K. *et al.* Random access quantum information processors using multimode circuit quantum electrodynamics. *Nature Communications* **8** (2017).
[48] Gao, Y. Y. *et al.* Programmable interference between two microwave quantum memories. *Phys. Rev. X* **8**, 021073 (2018).
[49] Place, A. P. M. *et al.* New material platform for superconducting transmon qubits with coherence times exceeding 0.3 milliseconds. *arXiv:2003.00024* (2020).

Acknowledgements

We thank C. Hann for discussions. We gratefully acknowledge the support provided by the Heising-Simons Foundation. This work made use of the Pritzker Nanofabrication Facility of the Institute for Molecular Engineering at the University of Chicago, which receives support from Soft and Hybrid Nanotechnology Experimental (SHyNE) Resource (NSF ECCS-1542205), a node of the National Science Foundation's National Nanotechnology Coordinated Infrastructure. This manuscript has been authored by Fermi Research Alliance, LLC under Contract No. DE-AC02-07CH11359 with the U.S. Department of Energy, Office of Science, Office of High Energy Physics, with support from its QuantISED program. We acknowledge support from the Samsung Advanced Institute of Technology Global Research Partnership.

Author Contributions

A.V.D, D.I.S, and A.C. conceived of the experiment. S.C. fabricated the device with assistance from A.V.D. The experiment was designed and conducted by A.V.D. with assistance from S.C., K.H., A.A., and R.K.N. Analysis was performed by A.V.D. All authors contributed to the preparation of the manuscript.

Competing Interests

The authors declare no competing interests.

Additional Information

Supplementary Information is available for this paper at.

Correspondence and requests for materials should be addressed to avdixit@uchicago.edu.